Itinerant-Electron Magnetism: The Importance of Many-Body Correlations

Markus Holzmann
Univ. Grenoble Alpes, CNRS, LPMMC, 38000 Grenoble, France
and Institut Laue Langevin, BP 156, F-38042 Grenoble Cedex 9, France

Saverio Moroni
CNR-IOM DEMOCRITOS, Istituto Officina dei Materiali, and SISSA Scuola Internazionale Superiore di Studi Avanzati, Via Bonomea 265, I-34136 Trieste, Italy

(Received 8 October 2019; accepted 5 May 2020; published 21 May 2020)

Do electrons become ferromagnetic just because of their repulsive Coulomb interaction? Our calculations on the three-dimensional electron gas imply that itinerant ferromagnetism of delocalized electrons without lattice and band structure, the most basic model considered by Stoner, is suppressed due to many-body correlations as speculated already by Wigner, and a possible ferromagnetic transition lowering the density is precluded by the formation of the Wigner crystal.

DOI: 10.1103/PhysRevLett.124.206404

In 1929, Bloch addressed the possibility of itinerant ferromagnetism [1] where the same electrons forming the conducting state give also rise to ferromagnetism. Considering the free homogeneous electron gas (jellium) as a minimal model to describe electrons in a metal, he concluded that the exchange energy may lead to a ferromagnetic state at densities slightly below those occurring in alkali metals. Considering correlation between positions of electrons with antiparallel spin, Wigner [2,3] approximately calculated the correlation energy—the gain of energy compared to the Hartree-Fock approximation—and pointed out the possibility of crystalline order at low densities. In the same paper [2], he also anticipated that the magnitude of the correlation energy is important for questions of para- and ferromagnetism modifying Bloch's theory on itinerant magnetism. Later, Stoner [4] predicted the occurrence of a continuous transition between zero and full magnetization at zero temperature introducing a repulsive energy term between opposite spin electrons to phenomenologically account for correlation effects. The threshold of the ratio between this repulsive interaction constant and the Fermi energy is now commonly known as the Stoner criterion.

The question whether pure Coulomb interactions between electrons can drive a magnetization transition without accompanying structural changes has a long and controversial history, starting from Bloch's prediction [1]. Based on the Hartree-Fock approximation, he considered the possibility of a first order (discontinuous) transition to a fully polarized, ferromagnetic electron liquid for electronic densities n, slightly lower than those of alkaline metals, $r_s \equiv a/a_B > 5.45$, where a_B is the Bohr radius and $a = (4\pi n/3)^{-1/3}$ is the mean electron distance. The first variational Monte Carlo (VMC) calculations [5] taking into account electron correlations without relying on perturbative high or low density expansions indicated a totally polarized quantum fluid for $r_s > 26(5)$ before the occurrence of a Wigner crystal at $r_s = 67(5)$. More accurate calculations based on fixed-node diffusion Monte Carlo (DMC) and transient estimates releasing the nodal constraint subsequently shifted the ferromagnetic liquid to lower densities [6,7], $75(5) < r_s < 100(20)$. Later calculations [8] predicted a partial polarization of up to 50% in the range $20 \lesssim r_s \lesssim 100$. Two decades later, new calculations [9] with larger system sizes observed a continuous transition from the paramagnetic to the ferromagnetic fluid around $r_s = 20(5)$ reaching full polarization around $r_s = 40(5)$ before freezing at $r_s = 65(10)$. The most recent quantum Monte Carlo (QMC) calculations [10], reducing systematic errors of the thermodynamic limit extrapolation and of the fixed-node bias, again support Stoner's picture of a continuous magnetic transition, but with an onset of partial spin polarization at $r_s = 50(2)$ and completion of full polarization at $r_s \approx 100$, just before Wigner crystallization which is estimated to occur at $r_s = 106(1)$ in Ref. [11].

Physical realization of such low density electron liquids at low temperatures is extremely challenging, and experimental findings [12] are controversial due to finite temperature and band structure effects [13,14]. Recent experimental efforts have been devoted to realize Stoner's model within ultracold atomic gases [15,16], where the interaction between two fermions is essentially described by momentum and energy independent s-wave scattering. However, there, the strong repulsive s-wave interaction is intrinsically connected with a short range interparticle bound state leading to molecule formation. Although local spin correlations have been observed, the interpretation of the experimental observations is not straightforward.

In this Letter, we show that Stoner's instability is precluded by the transition to the Wigner crystal and argue that itinerant magnetism is quite generally suppressed by correlation effects in the ground state of homogeneous quantum fluids with spin-independent repulsive interactions. Specifically, we present new results for jellium in three dimensions based on a sequence of wave functions featuring iterative backflow transformations [17,18] within the variational and the more accurate fixed-phase diffusion Monte Carlo methods [19,20]. Zero-variance extrapolation [17] of the ground state energies at finite system size allows us to reliably control the remaining, systematic bias of the fixed-phase DMC calculations. Finite-size corrections due to single-particle shell effects [21] and two-body terms [22–24] are applied for thermodynamic limit extrapolation. Improved accuracy proves crucial, as our calculations show that many-body correlations of the ground state wave function favor the unpolarized phase of the electron liquid compared to partial or fully polarized states and eventually prevent itinerant magnetism in jellium at any densities above crystallization. We also update the density of the transition to the Wigner crystal to a slightly lower value, $r_s = 113(2)$.

Methodological and computational improvements of the accuracy of QMC calculations thus seem to parallel the historical developments on the two-dimensional electron gas. The first QMC results [5,25] indicated an intermediate region with a fully polarized liquid ground state, shrinking, subsequently, to a weakly first-order polarization transition occurring just before Wigner crystallization [26,27], and, finally, disappearing completely [28] following improvements to the fixed node bias and finite-size methodology.

Taking further into account the absence of a polarized phase in ^{3}He, a strongly correlated Fermi liquid with an effective dominant hard-core interaction, we arrive at the quite general conclusion that pure correlation effects in homogeneous quantum liquids tend to suppress itinerant magnetization, in contrast to common argumentations based on Stoner's model. In these systems, crystallization, the spontaneous breaking of translational symmetry, seems to win the competition against spontaneous magnetization.

In the following, we describe the details of our numerical methods to determine the low-density ground state phase diagram of jellium–nonrelativistic electrons interacting via Coulomb's potential with each other and with a homogeneous positive background to guarantee charge neutrality [29,30]. The ground state energy per electron of the model at three values of the electronic density n, corresponding to $r_s = 70$, 100, and 120, and six different spin polarizations $\zeta = 0.0$, 0.18, 0.42, 0.61, 0.79, and 1.0, is addressed by variational and diffusion Monte Carlo simulations [19] of a finite system containing $N = 66$ electrons imposing periodic boundary conditions for the particles' positions; the long-range Coulomb potential is evaluated by standard splitting into real and reciprocal space contributions [31,32].

In the DMC runs [33], the number of walkers is 1280 and the time step is 15, 20, and 30 Ry^{-1} for $r_s = 70$, 100, and 120, respectively. The estimated time step error is 10^{-7} Ry or less, which is about the size of the statistical error on our final results (the zero-variance extrapolation of the DMC energy, see below). The population control bias is even smaller, of the order of 10^{-8} Ry.

The accuracy of the ground state energy of a finite system is limited by the underlying many-body trial wave function Ψ used for calculating expectation values in VMC [19] and for imposing the phase in DMC [20], respectively. In order to remove such a bias, we consider a series of trial wave functions of increasing quality, starting from the standard Jastrow-Slater and backflow forms (SJ and BF0) [10], and adding up to four iterative backflow transformations (BF1, …, BF4) [17].

Specifically, the Jastrow-Slater wave function SJ($\mathbf{R}$) explicitly depends on the coordinates $\mathbf{R}$ of all the particles through the two-body pseudopotential u_0 in the Jastrow factor $\exp[-U_0(\mathbf{R})]$, and through plane-wave orbitals in the Slater determinant $D(\mathbf{R})$. We then recursively build sets of transformed coordinates $\mathbf{Q}_0, \ldots, \mathbf{Q}_k$, where $\mathbf{Q}_i$ depends on $\mathbf{Q}_{i-1}$ through the ith backflow pseudopotential η_i, with $\mathbf{Q}_{-1} \equiv \mathbf{R}$. The kth iterative backflow wave function is

$$\mathrm{BF}k(\mathbf{R}) = \exp[-U_0(\mathbf{Q}_{-1}) - \cdots - U_k(\mathbf{Q}_{k-1})]D(\mathbf{Q}_k). \quad (1)$$

For the backflow wave functions we include both two- and three-body pseudopotentials u_0 and ξ_0 in $\exp(-U_0)$, and only two-body pseudopotentials u_i in $\exp(-U_i)$ for $i = 1, \ldots, k$. The plane-wave orbitals in the Slater determinant are evaluated at the last set of transformed coordinates, $\mathbf{Q}_k$.

The two-body pseudopotential u_0 is initially of the RPA form [5] with an explicit long-range part in Fourier space spanning the first 20 shells of reciprocal vectors, and the real-space part represented by locally piecewise-quintic Hermite interpolants (LPQHI) with 8 degrees of freedom, which are subsequently treated as optimization parameters. The three-body pseudopotential (ξ_0), the backflow pseudopotentials (η_i with $i = 0, \ldots, k$), and the two-body pseudopotentials in the transformed coordinates (u_i with $i = 1, \ldots, k$) are all expressed as LPQHI with 6 degrees of freedom each, with the exception of η_0 which is augmented with 5 shells of Fourier components. The LPQHI coefficients of all the pseudopotentials, as well as the Fourier components of η_0, are optimized independently for each wave function in the hierarchy.

The energy E computed for $r_s = 100$ in VMC and DMC simulations using all the above wave functions is plotted in Fig. 1 against the corresponding VMC variance $\sigma^2 = \langle\Psi|(H - \langle\Psi|H|\Psi\rangle)^2|\Psi\rangle$. The exact ground-state energy, which has zero variance, can be reliably estimated by extrapolation [17], given the smoothness of the data over a significant range extending to very low values of σ^2. We assume a quadratic dependence of E on σ^2. Since the range of validity of such a dependence is not known, we perform the

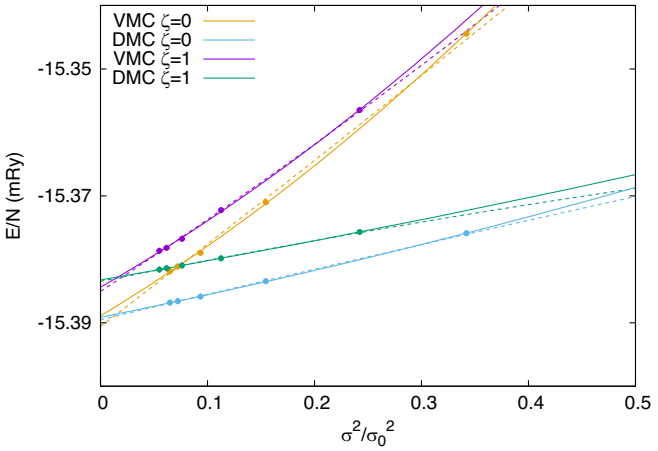

FIG. 1. Extrapolation of the energy to zero variance for $r_s = 100$ at polarizations $\zeta = 0$ and 1. The data are calculated with VMC and DMC using SJ, BF0, …, BF4 wave functions in order of decreasing energy. The reference value σ_0^2 is the variance of the local energy at $\zeta = 0$ with the SJ wave function. The curves are quadratic fits; for each set of data points (VMC and DMC for $\zeta = 0$ and 1) there are two curves, one of which (solid line) excludes the SJ energy from the fit.

extrapolation with and without the highest energies and variances, obtained with the SJ wave function. The result does not change significantly if we include the SJ result and/or switch between VMC and DMC data for the extrapolation. In particular, Fig. 2 shows that the polarization energy is only marginally influenced by the choice of the dataset.

Twist-averaged boundary conditions [21,33] are used to reduce shell effects of the finite simulation cell and afford thermodynamic limit extrapolation without resorting to large simulation cells. Residual single particle shell effects due to the discrete twist grid and to reduced-symmetry open-shell fillings for finite polarizations with $N = 66$, ΔT_0, are estimated from the noninteracting electron gas.

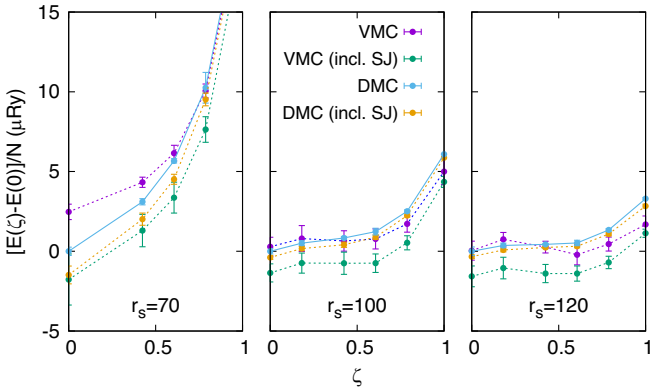

FIG. 2. The polarization energy $E(\zeta) - E(0)$ obtained from zero-variance extrapolations of the VMC and DMC energies, including or excluding the SJ result. The common reference energy $E(0)$ is the zero-variance extrapolation of the DMC energy without the SJ data.

Two-particle finite-size corrections for the potential and kinetic energy, ΔFSE, are addressed by interpolation of the long-range part of the static structure factor and by the analytical long-range expressions for the two-body and backflow pseudopotentials u_0 and η_0 of the wave function [23,34,35]. In contrast to the high density limit [36,37], where residual size effects in the kinetic energy introduce quasirandom fluctuations in the extrapolation, these effects are suppressed in the large r_s region addressed here (see Supplemental Material [33]). Furthermore, at low densities, the corrections ΔFSE are largely dominated by the zero-point energy of the plasmon [22]. Whereas the single particle size corrections depend on the spin polarization, the long-range structure factor does not reveal any systematic dependence on ζ within the statistical error of the present simulations. Therefore, we average the structure factor over spin polarizations in the calculation of ΔFSE, so that the final polarization energy is not affected by statistical fluctuations in the estimates of ΔFSE. Only the absolute value of the estimated ground state energy, used below to locate the Wigner crystallization, is then susceptible to the details of the calculation of ΔFSE.

The results for the energies and the variances obtained with different trial wave functions, the zero-variance extrapolations, and the finite-size corrections are collected in the Supplemental Material [33]. Note that the variance extrapolation is done on the energies of the finite-size system, and size corrections (for the polarization energy and the Wigner crystallization) are applied afterwards, using the value of ΔFSE obtained at the highest wave function level.

The final polarization energy of jellium at low densities, our main result, is shown in Fig. 3 for $r_s = 70$, 100, and 120. It is obtained from the zero–variance extrapolation of the DMC energy, excluding the SJ result. This choice gives the smoothest polarization energy, as well as the lowest χ^2 in the fit to the energy vs variance data, but it is otherwise uninfluential for the oucome that $E(\zeta)$ is higher than $E(0)$ for all the densities considered, and therefore a partially or fully polarized state is never stable. Confidence levels for our conclusion are given in the Supplemental Material [33].

The zero-variance extrapolation of the DMC energy, corrected for finite-size effects, is compared in Fig. 4 with the fixed-node DMC energy [19] of the Wigner crystal of Ref. [11] as a function of r_s. For the crystal phase, finite-size effects are assessed using large simulation cells with up to 512 electrons [11]. This procedure differs from that used in the present work for the liquid phase, but it should be equally reliable. The fixed-node DMC bias [19] for the crystal phase is negligible: it is bounded by (and presumably much smaller than) the difference between the fixed-node energy and the exact bosonic ground-state energy, which we find to be of the order of the statistical error on the crystal data of Fig. 4. The critical value for the Wigner crystallization is shifted to $r_s = 113(2)$, where the

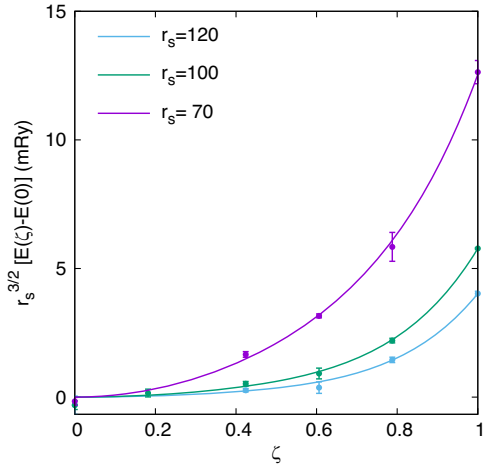

FIG. 3. The polarization energy $E(\zeta) - E(0)$ obtained from zero-variance extrapolations of the DMC energies without the SJ result. The lines are polynomial fits with terms of order 0, 2, and 6. Alternative functional forms and ensuing confidence levels for our conclusions are discussed in the Supplemental Material [33].

uncertainty includes both the statistical error of the simulation data and a conservative estimate of the residual bias in the size corrections [33].

In this Letter, we have presented accurate quantum Monte Carlo calculations addressing the possibility of a magnetically polarized fluid in the ground state phase diagram of the homogeneous electron gas. We have shown that iterated backflow wave functions [17,18] provide highly accurate results for the energy and very low values of its variance, such that a zero variance extrapolation provides fairly unbiased results for the polarization energy. Our calculations clearly demonstrate that the simple mean-field picture based on Stoner's model is not sufficient to explain itinerant ferromagnetism as the partially or fully polarized fluid state is unstable versus Wigner crystallization.

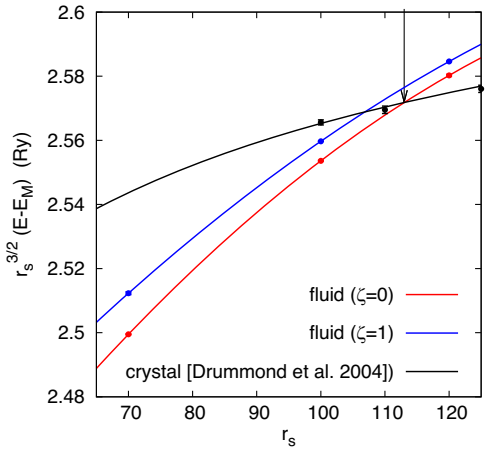

FIG. 4. DMC energy as a function of r_s for the paramagnetic and the ferromagnetic fluid and for the Wigner crystal. $E_M = -1.79186/r_s$ Ry is the Madelung energy of the bcc lattice [11]. The lines are quadratic interpolations for the fluid phases, and a fit of the form [11] $a + b/\sqrt{r_s}$ for the Wigner crystal. The arrow at $r_s = 113$ locates the crystallization point.

Therefore, in addition to repulsive interparticle interactions, band structure effects must play an essential role for the occurrence of itinerant ferromagnetism in real materials.

Similar results have been found for liquid ^{3}He in two [17,38] and three dimensions [18,39], the two-dimensional electron gas [28], and two-dimensional quantum gases with repulsive dipolar interaction [40], where accurate, quantitative treatment of correlation effects have always stabilized the spin-unpolarized phase.

From a more general point of view, Stoner's instability constitutes a reconstruction of the Fermi surface of the unpolarized to the polarized gas due to interactions. However, this instability is quite naturally in competition with the reconstruction of the Fermi surface related to spin and charge density waves [41–43] (not addressed in this work) or Brillouin zone formation for Wigner crystallization. Despite the quite different interparticle interaction, hard or soft core potentials, the Stoner transition to a spin-polarized phase predicted within mean-field arguments seems to be quite generally preceded by transition to a crystalline phase for homogeneous systems with spin-independent interactions.

We acknowledge the CINECA award under the ISCRA initiative for the availability of high performance computing resources and the Fondation NanoSciences (Grenoble) for support. Part of the computations were performed using the Froggy platform of the CIMENT infrastructure, which is supported by the Rhône-Alpes region (Grant No. CPER07-13 CIRA) and the project Equip@Meso (ANR-10-EQPX-29-01) of the ANR.

[1] F. Bloch, Z. Phys. **57**, 545 (1929).
[2] E. P. Wigner, Phys. Rev. **46**, 1002 (1934).
[3] E. P. Wigner, Trans. Faraday Soc. **34**, 678 (1938).
[4] E. C. Stoner, Proc. R. Soc. A **165**, 372 (1938).
[5] D. Ceperley, Phys. Rev. B **18**, 3126 (1978).
[6] D. M. Ceperley and B. J. Alder, Phys. Rev. Lett. **45**, 566 (1980).
[7] D. M. Ceperley and B. J. Alder, J. Phys. C **41**, 295 (1980).
[8] B. J. Alder, D. M. Ceperley, and E. L. Pollock, Int. J. Quantum Chem. **22**, 49 (1982).
[9] G. Ortiz, M. Harris, and P. Ballone, Phys. Rev. Lett. **82**, 5317 (1999).
[10] F. H. Zong, C. Lin, and D. M. Ceperley, Phys. Rev. E **66**, 036703 (2002).
[11] N. D. Drummond, Z. Radnai, J. R. Trail, M. D. Towler, and R. J. Needs, Phys. Rev. B **69**, 085116 (2004).
[12] D. P. Young, D. Hall, M. E. Torelli, Z. Fisk, J. L. Sarrao, J. D. Thompson, H.-R. Ott, S. B. Oseroff, R. G. Goodrich, and R. Zysler, Nature (London) **397**, 412 (1999).

[13] S. Ichimaru, Phys. Rev. Lett. **84**, 1842 (2000).
[14] G. Ortiz, M. Harris, and P. Ballone, Phys. Rev. Lett. **84**, 1843 (2000).
[15] G.-B. Jo1, Y.-R. Lee, J.-H. Choi, C. A. Christensen, T. H. Kim, J. H. Thywissen, D. E. Pritchard, and W. Ketterle, Science **325**, 1521 (2009).
[16] G. Valtolina, F. Scazza, A. Amico, A. Burchianti, A. Recati, T. Enss, M. Inguscio, M. Zaccanti, and G. Roati, Nat. Phys. **13**, 704 (2017).
[17] M. Taddei, M. Ruggeri, S. Moroni, and M. Holzmann, Phys. Rev. B **91**, 115106 (2015).
[18] M. Ruggeri, S. Moroni, and M. Holzmann, Phys. Rev. Lett. **120**, 205302 (2018).
[19] L. K. Wagner and D. M. Ceperley, Rep. Prog. Phys. **79**, 094501 (2016).
[20] G. Ortiz, D. M. Ceperley, and R. M. Martin, Phys. Rev. Lett. **71**, 2777 (1993).
[21] C. Lin, F.-H. Zong, and D. M. Ceperley, Phys. Rev. E **64**, 016702 (2001).
[22] S. Chiesa, D. M. Ceperley, R. M. Martin, and M. Holzmann, Phys. Rev. Lett. **97**, 076404 (2006).
[23] M. Holzmann, R. C. Clay III, M. A. Morales, N. M. Tubman, D. M. Ceperley, and C. Pierleoni, Phys. Rev. B **94**, 035126 (2016).
[24] N. D. Drummond, R. J. Needs, A. Sorouri, and W. M. C. Foulkes, Phys. Rev. B **78**, 125106 (2008).
[25] F. Rapisarda and G. Senatore, Aust. J. Phys. **49**, 161 (1996).
[26] D. Varsano, S. Moroni, and G. Senatore, Europhys. Lett. **53**, 348 (2001).
[27] C. Attaccalite, S. Moroni, P. Gori-Giorgi, and G. B. Bachelet, Phys. Rev. Lett. **88**, 256601 (2002).
[28] N. D. Drummond and R. J. Needs, Phys. Rev. Lett. **102**, 126402 (2009).
[29] G. F. Giuliani and G. Vignale, *Quantum Theory of the Electron Liquid* (Cambridge University Press, Cambridge, England, 2005).
[30] R. M. Martin, L. Reining, and D. M. Ceperley, *Interacting Electrons* (Cambridge University Press, Cambridge, England, 2016).
[31] P. P. Ewald, Ann. Phys. (Berlin) **369**, 253 (1921).
[32] V. Natoli and D. M. Ceperley, J. Comput. Phys. **117**, 171 (1995).
[33] See Supplemental Material at http://link.aps.org/supplemental/10.1103/PhysRevLett.124.206404 for details of the simulations, interpolations of the polarization energy, finite-size corrections, and tables with all QMC data and their zero-variance extrapolations.
[34] M. Holzmann, D. M. Ceperley, C. Pierleoni, and K. Esler, Phys. Rev. E **68**, 046707 (2003).
[35] M. Holzmann, B. Bernu, and D. M. Ceperley, J. Phys. Conf. Ser. **321**, 012020 (2011).
[36] M. Ruggeri, P. López Ríos, and A. Alavi, Phys. Rev. B **98**, 161105(R) (2018).
[37] G. G. Spink, R. J. Needs, and N. D. Drummond, Phys. Rev. B **88**, 085121 (2013).
[38] M. Nava, A. Motta, D. E. Galli, E. Vitali, and S. Moroni, Phys. Rev. B **85**, 184401 (2012).
[39] M. Holzmann, B. Bernu, and D. M. Ceperley, Phys. Rev. B **74**, 104510 (2006).
[40] T. Comparin, R. Bombin, M. Holzmann, F. Mazzanti, J. Boronat, and S. Giorgini, Phys. Rev. A **99**, 043609 (2019).
[41] A. W. Overhauser, Phys. Rev. Lett. **4**, 462 (1960); Phys. Rev. **128**, 1437 (1962).
[42] F. Delyon, B. Bernu, L. Baguet, and M. Holzmann, Phys. Rev. B **92**, 235124 (2015).
[43] D. Gontier, C. Hainzl, and M. Lewin, Phys. Rev. A **99**, 052501 (2019).